Variable Conductance Heat Pipe Performance Analysis: Zero-to-Full Load

Richard P. Bobco*
Hughes Aircraft Company, Los Angeles, California

Test data for an aluminum/ammonia/nitrogen variable conductance heat pipe (VCHP) with a central core wick are presented and used to develop an analytical model for predicting evaporator temperature as a function of heat load and environmental conditions. These data show that VCHP performance at very low heat loads is dominated by heat losses from the so-called primary adiabatic section. The present formulation is an extension of an earlier VCHP model that was found suitable for engineering calculations over a heat-load range of about 20–100% of full load; the extended model presented here includes the operating range of 0–100% of full heat load. The extended model postulates a uniform condensation flux q_0 in the nonadiabatic transport section, and a second but different uniform condensation flux q_1 in the active condenser. A set of nonlinear, transcendental, algebraic equations describes the performance of a simple VCHP. An incomplete definition of the two condensation fluxes requires a double-iteration procedure with respect to q_0 and ℓ_c to solve the set of equations. A comparison of analytical temperature distributions and experimental data points shows that the present model is adequate for most engineering applications.

Nomenclature

A_c = internal cross-section area for vapor/gas transport
A_r = reservoir surface area for heat transfer
A_w = conduction cross section of wick plus wall
c = local molar density of vapor and noncondensable gas mixture
D = local diffusion coefficient of vapor/gas mixture
h = local heat-loss coefficient (convection plus linearized radiation)
H = local latent heat of vaporization
k_w = thermal conductivity of pipe wall and wick structure
ℓ = axial length
ℓ_c = condensation front location
L_j = nondimensional length, ℓ_j/ℓ_3
m_g = mass of noncondensable gas
M_v = vapor molecular weight
p_g = gas partial pressure
p_v = vapor partial pressure
q_0 = condensation heat flux in primary transport section
q_1 = condensation heat flux in active condenser section
Q = heat load leaving evaporator
Q_{in} = experimental gross input power to evaporator
Q_r = heat load to reservoir
R_g = gas constant
S = pipe periphery
T = local axial temperature
T_s = local environment (sink) temperature
U = overall heat-transfer coefficient
V_c = volume occupied by vapor/gas, $A_c\ell_3$
V_r = reservoir volume
z = axial location
Z = real gas compressibility factor
ζ = nondimensional axial location, z/ℓ_3
ψ = gas density parameter
$(\tilde{\ })$ = condition when $L_c = L_1$
$(\ )_0$ = condensing subregion of primary transport section
$(\ )_1$ = noncondensing subregion of primary transport section or active condenser section
$(\ )_2$ = inactive condenser section
$(\ )_3$ = secondary transport section
$(\ )_c$ = condensation front
$(\ )'_c$ = condensation front based on single-flux model[1]
$(\ )_e$ = evaporator
$(\ )'_F$ = full load condition based on $L_c = L_2$ and single-flux model[1]
$(\ )_r$ = reservoir
$(\ )_t$ = transition between necessary double-flux model and optional single-flux model[1]

Presented as Paper 87-1614 at the AIAA 22nd Thermophysics Conference, Honolulu, HI, June 8–10, 1987; received Nov. 2, 1987; revision received Feb. 15, 1988.

*Senior Scientist. Associate Fellow AIAA.

Introduction

A SIMPLIFIED analytical model of a variable conductance heat pipe (VCHP) suitable for making performance predictions for many engineering applications was described in 1987.[1] A set of simultaneous, nonlinear, transcendental, algebraic equations was derived that requires a numerical solution to find evaporator temperature as a function of heat load with geometry, environmental conditions, and thermophysical properties as parameters. The formulation was validated by comparing the performance predictions with both test data and a more rigorous analysis reported by Edwards and Marcus.[2] The simplified formulation was found to be adequate for heat loads in the range of 20–100%, but not suitable for either very low heat loads (0–20%) or excessive heat loads (>100%). The emphasis in the present study is on very low to moderate heat loads that are important in space applications where power consumption must be minimized and heat pipe freezing avoided.

The work reported here describes experimental and analytical studies leading to an extended first-order analytical model capable of predicting VCHP performance over the heat load range 0–100%. This paper contains descriptions of the VCHP test program, analyses, model validation, and a numerical example that illustrates the use of the present model and delineates the scope of the earlier model.[1]

VCHP Tests

The tested VCHP was an aluminum pipe (6061-T6), 1.27 o.d. × 0.071 wall × 194.0 cm long, with a stainless steel reservoir (304 L, 252.4 cm^3 volume). The wick was tailored to accommodate two pipe bends of 80 and 74 deg, respectively, and included various combinations of a central core knitted mesh (5056 aluminum), wall screen (120 mesh, 304 stainless

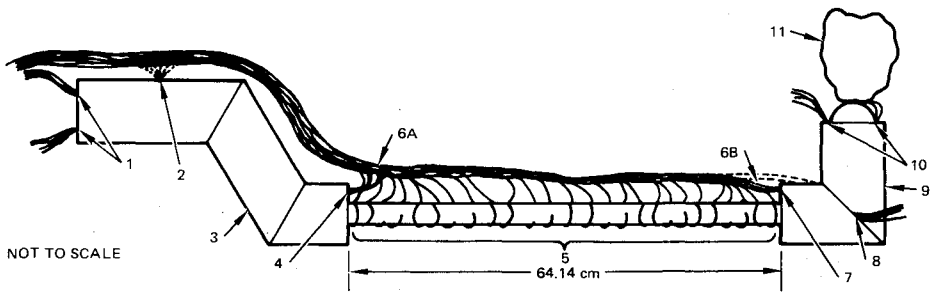

1) 7 TCs AND 4 HEATER WIRE LEADS FROM SYNTACTIC FOAM
2) 12 TCs AND 4 HEATER WIRE LEADS FROM GUARD HEATED ALUMINUM TUBE AT EVAPORATOR/PRIMARY TRANSPORT INTERFACE
3) 7.62 cm OD ALUMINUM TUBE (AS RECEIVED) WITH 3 HELICAL WOUND GUARD HEATER CIRCUITS (1 EVAPORATOR, 2 PRIMARY TRANSPORT SECTIONS)
4) 4 TCs FROM SYNTACTIC FOAM
5) 1.27 cm OD BLACK PAINTED CONDENSER CYLINDER WITH 26 TCs BONDED TO SURFACE (EACH TC WINDS AROUND CYLINDER BY SINGLE HELIX TO MINIMIZE CONDUCTION LOSS AT JUNCTION)
6) (A) TC WIRE BUNDLE DIAMETER APPROXIMATELY 0.84 cm AT PRIMARY TRANSPORT/CONDENSER INTERFACE
(B) WIRE BUNDLE DIAMETER APPROXIMATELY 0.635 cm AT CONDENSER/SECONDARY TRANSPORT INTERFACE
7) 15 TCs FROM SYNTACTIC FOAM REMOVING ENERGY FROM SECONDARY TRANSPORT SECTION AND RESERVOIR
8) 4 HEATER WIRES FROM ALUMINUM TUBE AT 2nd TRANSPORT/RESERVOIR INTERFACE
9) 7.62 cm OD ALUMINUM TUBE OVER SECONDARY TRANSPORT SECTION AND RESERVOIR; NO GUARD HEATERS
10) 2 RESERVOIR TCs AND 4 RESERVOIR HEATER LEADS FROM SYNTACTIC FOAM
11) HEAT PIPE FILL TUBE AND VALVE ENCLOSED IN MLI BLANKET (10 LAYERS)

GENERAL: THERMOCOUPLES 30 GAUGE DUPLEX COPPER CONSTANTAN IN KAPTON INSULATION; HEATER WIRE LEADS 22 GAUGE COPPER IN PLASTIC INSULATION

Fig. 1 Unfinned VCHP schematic and data reduction heat-balance considerations.

steel screen), and spacer wicks in the several pipe sections. An aluminum/stainless steel transition section (1.27 o.d. × 0.071 cm thick × 8.89 cm long) connected the pipe to the gas reservoir. The working fluid and noncondensable gas were ammonia (NH_3) and nitrogen (0.14 g/mole, N_2), respectively. The pipe was manufactured by the Hughes Electron Dynamics Division, Torrance, California.

The evaporator length was 52.1 cm at the end of the pipe opposite the reservoir, and was wound with electrical resistance heating tape (Clayborn Labs Inc.) 1.27 cm wide with four conductors. The primary transport section length was 73.81 cm, followed by the condenser (64.14 cm); the second transport section was 12.85 cm. The two bends introduced an uncertainty of approximately ±1.27 cm in the length of the primary transport section and the overall length of the pipe. A stainless steel fill tube (0.635 o.d. × 6.35 cm long) and needle valve were attached to the top of the reservoir. The evaporator, primary transport section, condenser, and secondary transport section were coplanar; the reservoir cylindrical axis was perpendicular to the VCHP plane.

Fifty-nine thermocouples (TC) (30-gage, copper-constantan) were bonded to the pipe surface along its length; 13 additional thermocouples were bonded to the reservoir surface. The thermocouple adhesive was Eccobond, a silver-loaded epoxy. After the heater tape and thermocouples were installed, the evaporator, both transport sections, and most of the reservoir were enclosed by lengths of 7.62 o.d. × 0.079 cm thick wall aluminum tube. The annular cavity between the pipe or reservoir surface and the aluminum tube case was filled with syntactic foam (Bisphenol A with microballoons 641 kg/m^3, k(foam) ≈ 0.073 W/m-K). Electrical heating tape was bonded to the outside of the aluminum tube to create three independently controlled guard heaters (one evaporator guard, two primary transport guards). The instrumentation was completed by bonding additional thermocouples to the outside of the aluminum tube case (TC) [evaporator (6 TC's), primary transport (9 TC's), secondary transport (1 TC), and reservoir (8 TC's)]. A schematic of the test configuration is shown in Fig. 1.

The heat pipe was suspended in a near-horizontal orientation (~1.91 cm adverse tilt) in an open-top cylindrical chamber and tested in air with walls at laboratory temperature. Eighteen TC's were used to measure the air temperature in the plane of the heat pipe. Data acquisition was provided by the Hughes VIDAR system. All TC readings and heater loads were recorded at 15-min intervals. After setting the evaporator heat load, each test condition was run for 2–3 h to adjust

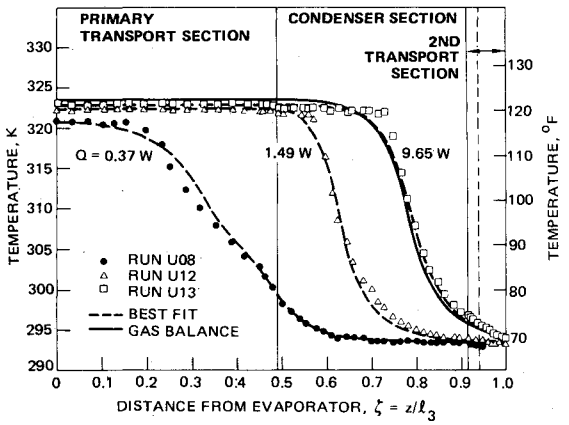

a) Operating at very low, low, and moderate heat loads—test data and analytical results

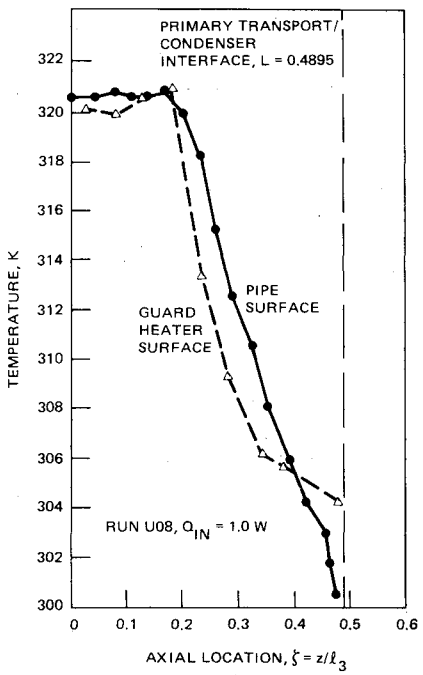

b) Surface and guard heater at very low heat loads (test data only)

Fig. 2 VCHP experimental and analytical axial temperatures.

Table 1 Analytical input data based on experimental data

Run	U08	U12	U13
Q_{in}, W	1.0	5.1	10.2
T_e, K	320.6	322.4	322.8
Q[a], W	0.369	4.587	9.649
T_{s0}, K	318.3	322.4	322.8
T_{s1}, K	305.0	293.7	293.8
T_{s2}, K	293.6	293.7	293.8
T_{s3}, K	293.6	293.7	293.8
T_{sr}, K	293.6	293.7	293.8
U_0, W/m^2-K	6.42 (6.81)[b]	6.42 (6.81)[b]	6.42 (6.81)[b]
U_1, W/m^2-K	6.42 (6.81)[b]	N/A	N/A
h_1, W/m^2-K	N/A	18.34	18.40
h_2, W/m^2-K	10.90	14.48	12.27
U_3, W/m^2-K	6.42 (6.81)[b]	6.42 (6.81)[b]	6.42 (6.81)[b]
U_r[c], W/m^2-K	11.36	11.36	11.36
Q_r, W	0	0	0
L_c nondimensional[d]	0.32 (0.3157)[d]	0.62 (0.6237)[d]	0.79 (0.788)[d]
$\ell_1 = 0.7382$ m	$\ell_2 = 1.380$ m	$\ell_3 = 1.508$ m	
$S = 0.0399$ m	$A_w = 2.678$ E-5 m^2	$A_c = 3.206$ E-6 m^2[e]	
$A_r = 1.579$ E-3 m^2[c]	$V_r = 2.524$ E-4 m^3[e]	$m_g = 3.921$ E-3 kg[e]	
$R_g = 0.2968$ kJ/kg-K	$k_w = 171.3$ w/m-K		

[a]Corrected for losses in evaporator section. [b]Empirical value for best fit to test data. [c]Estimated, precise value not available. [d]Estimated from XP temperature profile. [e]Manufacturer's data.

guard heaters and reach a steady state. A total of 15 test runs were made in the air environment, but only three runs are reported here.

These three test runs were in the very low-to-middle heat-load range. The power levels to the evaporator heater were as follows: run U08, 1.0 W; run U12, 5.1 W; run U13, 10.2 W. These runs were selected in part because the temperature data showed minimal temperature differentials along the length of the aluminum/stainless steel transition section. Axial temperature distributions are shown in Fig. 2. The heater power input Q_{in}, subsequently, was corrected for losses through the insulation, thermocouple leads, and heater leads to obtain the heat to the evaporator working fluid Q.

A detailed analysis of losses through insulation from TC wires and the exposed condenser surface led to the heat-loss coefficients summarized in Table 1. The film coefficients h_1 and h_2 at the condenser surface were found to be 12.8% higher than theoretical values[3] for the combined loss by natural convection and radiation from a horizontal cylinder; the disparity is attributed to the influence of TC's on the condenser surface. The 12.8% deviation between theoretical and observed external film coefficients provides a measure of the accuracy of the heat balance and data reduction process. The location of the condensation front $L_c = \ell_c/\ell_3$ was estimated from the axial temperatures; previously,[1] it was found that the condensation front occurs at an inflection point in the axial temperature distribution. The temperatures T_{s0}, T_{s1}, etc., are mean values of zonal sink temperatures. The guard-heated surfaces were nearly isothermal in runs U12 and U13, but not at all uniform in run U08. Figure 2b shows axial temperatures of the pipe surface and the guard-heated surface for run U08 in the primary transport section.

The heat-balance results appear to be credible despite small uncertainties in TC locations associated with the pipe bends and the thermal conductivity of the syntactic foam. The most significant observation made during the data reduction and analysis concerned the magnitude of heat losses in the evaporator and primary transport sections; sizable heat losses occurred in these sections despite the care taken in adjusting guard heater temperatures. The evaporator and transport section losses were most pronounced at very low heat loads. For example, in run U08 the heater power load was 1 W; however, after accounting for heat leaks through the insulation, TC leads, and heater power leads, it was found that only 0.37 W entered the primary transport section. It appears that at very low heat loads, VCHP performance is dominated by losses in the evaporator and primary transport sections. It was concluded that an analytical model of VCHP must account for losses in those sections to predict performance over the full range of heat loads.

Analysis

The first-order model described in Ref. 1 is based on several concepts that simplify the prediction of evaporator temperature as a function of heat load. The simplifications include the use of a uniform condensation flux, a noncondensable gas mass balance based on zonal mean temperatures, and a seemingly explicit expression for locating the position of the condensation front. The geometry and nomenclature are similar to those of Ref. 1. Assumptions are:

1) The coordinate system origin is at the interface between the evaporator and primary transport sections (Fig. 3).

2) Different sink temperatures are postulated for each of the five zones.

3) Imperfect insulation encloses the primary and secondary transport sections allowing radial heat losses from those regions.

4) The reservoir temperature T_r is uniform and has the same value as the end of the pipe [i.e., $T_r = T_3(\ell_3)$].

5) The condensation flux (i.e., heat release) is uniform within a zone, i.e., q_0 in $0 < z \le \ell_1$ and q_1 in $\ell_1 < z \le \ell_c$.

6) The wick extends the length of the heat pipe and into the reservoir.

7) Axial conduction is negligible at $z = 0$ (i.e., $dT/dz = 0$).

8) There is negligible gas in the region $z < 0$.

9) The vapor, gas, and structure (i.e., wick and wall) temperatures are identical at any axial location and in the resevoir.

10) The noncondensable gas behaves like a perfect gas $p_g V = m_g R_g T$.

11) Axial heat transfer occurs by conduction in the pipe wall; radial heat transfer occurs at both exposed and insulated surfaces ($0 < z \le \ell_3$) either by convection and/or linearized radiation.

12) The heat load and environmental conditions are steady.

13) Total pressure is constant everywhere in $0 < z \le \ell_3$ and in the reservoir. Additional assumptions are identified in the analysis below.

The equations required to formulate the problem follow below. The analytical model does not include the evaporator section. A separate heat-balance equation is required to relate

Table 2 Fin equation: zonal parameters $k_w A_w(d^2T/dz^2) - SU(z)[T - T_s(z)] = -Sq(z)$

	Very low heat loads $0 < \ell_c \le \ell$				Low-to-full heat loads $\ell_1 < \ell_c \le \ell_2$			
VCHP zone	Range	$U(z)$	$T_s(z)$	$q(z)$	Range	$U(z)$	$T_s(z)$	$q(z)$
Primary transport, condensing	$0 < z \le \ell_c$	U_0	T_{s0}	q_0	$0 < z \le \ell_1$	U_0	T_{s0}	q_0
Primary transport, noncondensing	$\ell_c < z \le \ell_1$	U_1	T_{s1}	0	—	—	—	—
Condenser, active	—	—	—	—	$\ell_1 < z \le \ell_c$	h_1	T_{s1}	q_1
Condenser, inactive	$\ell_1 < z \le \ell_2$	h_2	T_{s2}	0	$\ell_c < z \le \ell_2$	h_2	T_{s2}	0
Secondary transport	$\ell_2 < z \le \ell_3$	U_3	T_{s3}	0	$\ell_2 < z \le \ell_3$	U_3	T_{s3}	0

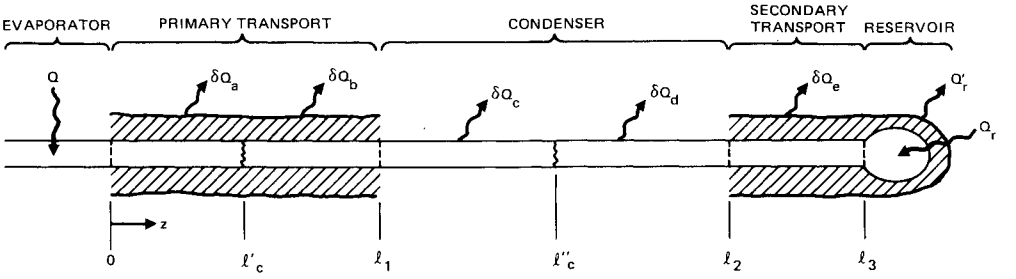

Fig. 3 Coordinate system and analytical zones for very low and low-to-full heat loads.

	VCHP SECTION	INTERVAL	HEAT LOSS COEFFICIENT	SINK TEMPERATURE	SURFACE HEAT LOSS
VERY LOW HEAT LOAD	PRIMARY TRANSPORT				
	CONDENSING	$0 < z \le \ell'_c$	U_0	T_{s0}	$\delta Q_a = \delta Q_0 = U_0 S\,[T_0(z) - T_{s0}]\,dz$
	NONCONDENSING	$\ell'_c < z \le \ell_1$	U_1	T_{s1}	$\delta Q_b = \delta Q_1 = U_1 S\,[T_1(z) - T_{s1}]\,dz$
	CONDENSER	$\ell_1 < z \le \ell_2$	h_2	T_{s2}	$\delta Q_c = \delta Q_d = \delta Q_2 = h_2 S\,[T_2(z) - T_{s2}]\,dz$
	SECONDARY TRANSPORT	$\ell_2 < z \le \ell_3$	U_3	T_{s3}	$\delta Q_e = \delta Q_3 = U_3 S\,[T_3(z) - T_{s3}]\,dz$
	RESERVOIR	$z > \ell_3$	U_r	T_{sr}	$Q_r = U_r A_r\,[T_r - T_{sr}]$
LOW-TO-FULL HEAT LOAD	PRIMARY TRANSPORT	$0 < z \le \ell_1$	U_0	T_{s0}	$\delta Q_a = \delta Q_b = \delta Q_0 = U_0 S\,[T_0(z) - T_{s0}]\,dz$
	CONDENSER ACTIVE	$\ell_1 < z \le \ell''_c$	h_1	T_{s1}	$\delta Q_c = \delta Q_1 = h_1 S\,[T_1(z) - T_{s1}]\,dz$
	INACTIVE	$\ell''_c < z \le \ell_2$	h_2	T_{s2}	$\delta Q_d = \delta Q_2 = h_2 S\,[T_2(z) - T_{s2}]\,dz$
	SECONDARY TRANSPORT	$\ell_2 < z \le \ell_3$	U_3	T_{s3}	$\delta Q_e = \delta Q_3 = U_3 S\,[T_3(z) - T_{s3}]\,dz$
	RESERVOIR	$z > \ell_3$	U_r	T_{sr}	$Q_r = U_r A_r\,[T_r - T_{sr}]$

the heat load entering the primary transport section to the power input to, and losses from, the evaporator. The equations appropriate to the primary transport section through the gas reservoir are presented below.

Fin Equation

$$k_w A_w \frac{d^2T}{dz^2} - SU(z)[T - T_s(z)] = -Sq(z) \tag{1}$$

Zonal values of heat-loss coefficient $U(z)$, environmental sink temperature $T_s(z)$, and condensation flux are summarized in Table 2. The boundary conditions at the two ends of the pipe are taken as 1) no axial conduction at the evaporator/primary transport interface ($z = 0$), and 2) a heat balance on the isothermal reservoir at the secondary transport/reservoir interface ($z = \ell_3$):

$$z = 0, \qquad \left.\frac{dT_0}{dz}\right|_0 = 0 \tag{2a}$$

$$z = \ell_3, \qquad -k_w A_w \left.\frac{dT_3}{dz}\right|_{\ell_3} = U_r A_r[T_3(\ell_3) - T_{sr}] - Q_r \tag{2b}$$

At the zonal interfaces $z = \ell_c, \ell_1, \ell_2$, matching conditions on temperature and flux are postulated:

$$z = \ell_i, \qquad T(\ell_i^-) = T(\ell_i^+), \qquad \left.\frac{dT}{dz}\right|_{\ell_i^-} = \left.\frac{dT}{dz}\right|_{\ell_i^+} \tag{3}$$

It should be observed that the pipe material and cross-sectional area are assumed to be uniform along the entire length, $0 < z \le \ell_3$. This condition did not exist in the tested heat pipe where a short tubular insert of low-thermal conductivity was used at one end of the secondary transport section. Such inserts may be accommodated in the analysis at the expense of mathematical complexity by introducing additional zonal fin equations.

Overall Heat Balance

It is postulated that all of the heat power entering the primary transport section is lost by condensation to the inner pipe surface; that is, the flow energy at the condensation front is negligible. This postulate implies the following conservation expressions:

Very low heat loads, $0 < \ell_c \le \ell_1$:

$$Q = q_0 S \ell_c \tag{4a}$$

Low-to-full heat loads, $\ell_1 < \ell_c \le \ell_2$:

$$Q = q_0 S \ell_1 + q_1 S(\ell_c - \ell_1) \tag{4b}$$

In Eq. (4b), the relationship between q_0 and q_1 is unspecified.

Noncondensable Gas Mass Balance

The location of the condensation front ℓ_c is unknown and must be found from the gas mass balance

$$m_g = \left(\frac{p_g V}{R_g T}\right)_r + A_c \int_0^{\ell_3} \frac{p_g\,dz}{R_g T} \tag{5}$$

where p_g is the local gas pressure.

Table 3 Local temperatures: zonal parameters $T_i(\zeta) = f_i(\zeta) + A_i \cosh b_i Z_i + B_i \sinh b_i Z$

	Very low heat loads $0 < L_c \le L_1$				Low-to-full heat loads $L_1 < L_c \le L_2$			
VCHP zone	Range	i	$f_i(\zeta)$	Z_i	Range	i	$f_i(\zeta)$	Z_i
Primary transport, condensing	$0 < \zeta \le L_c$	0	$T_{s0} + \frac{q_0}{U_0}$	ζ	$0 < \zeta \le L_1$	0	$T_{s0} + \frac{q_0}{U_0}$	ζ
Primary transport, noncondensing	$L_c < \zeta \le L_1$	1	T_{s1}	$(\zeta - L_c)$	——	——	——	——
Condenser, active	——	——	——	——	$L_1 < \zeta \le L_c$	1	$T_{s1} + \frac{q_1}{h_1}$	$(\zeta - L_1)$
Condenser, inactive	$L_1 < \zeta \le L_2$	2	T_{s2}	$(L_2 - \zeta)$	$L_c < \zeta \le L_2$	2	T_{s2}	$(L_2 - \zeta)$
Secondary transport	$L_2 < \zeta \le 1$	3	$T_{s3} + \lambda_3 \sinh b_3 \zeta$	$(1 - \zeta)$	$L_2 < \zeta \le 1$	3	$T_{s3} + \lambda_3 \sinh b_3 \zeta$	$(1 - \zeta)$

$$\lambda_3 = \frac{\hat{U}_r(T_{sr} - T_{s3}) + Q_r \ell_3 / k_w A_w}{b_3 \cosh b_3 + \hat{U}_r / \sinh b_3} \qquad \hat{U}_r = U_r A_r \ell_3 / k_w A_w$$

Table 4 Mean temperatures: zonal parameters $\bar{T}_i = \bar{f}_i + (1/b_i W_i)[A_i \sinh b_i W_i + B_i(\cosh b_i W_i - 1)]$

	Very low heat loads $0 < L_c \le L_1$				Low-to-full heat loads $L_1 < L_c \le L_2$			
VHCP zone	Range	i	$\bar{f}_i$	W_i	Range	i	$\bar{f}_i$	W_i
Primary transport, condensing	$0 < \zeta \le L_c$	0	$T_{s0} + \frac{q_0}{U_0}$	L_c	$0 < \zeta \le L_1$	0	$T_{s0} + \frac{q_0}{U_0}$	L_1
Primary transport, noncondensing	$L_c < \zeta \le L_1$	1	T_{s1}	$(L_1 - L_c)$	——	——	——	——
Condenser, active	——	——	——	——	$L_1 < \zeta \le L_c$	1	$T_{s1} + \frac{q_1}{h_1}$	$(L_c - L_1)$
Condenser, inactive	$L_1 < \zeta \le L_2$	2	T_{s2}	$(L_2 - L_1)$	$L_c < \zeta \le 1$	2	T_{s2}	$(L_2 - L_c)$
Secondary transport	$L_2 < \zeta \le 1$	3	$T_{s3} + \left(\frac{\lambda_3}{b_3 W_3}\right) x$ $(\cosh b_3 - \cosh b_3 L_2)$	$(1 - L_2)$	$L_2 < \zeta \le 1$	3	$T_{s3} + \left(\frac{\lambda_3}{b_3 W_3}\right) x$ $(\cosh b_3 - \cosh b_3 L_2)$	$(1 - L_2)$

Gas and Vapor Pressure Equations

The total pressure in the heat pipe and reservoir is virtually constant at all locations and has the magnitude of the vapor pressure in the evaporator $p_{tot} = p_v(T_e)$.[2,4] From the law of partial pressures, the local gas pressure follows as

$$p_g[T(z)] = p_v(T_e) - p_v[T(z)] \tag{6a}$$

Finally, the vapor pressures may be found from a correlation[5] of the form

$$p_v(T) = C \exp[f(T)], \qquad f(T) = \sum_{m=0}^{5} D_m T^m \tag{6b}$$

Temperatures and Condensation Front

Equations (1) and (5) must be solved simultaneously to obtain a formulation for predicting both evaporator temperature and condensation front location as a function of heat load Q. Equation (1) may be integrated to find a set of zonal local temperatures of the form

$$T_i(\zeta) = f_i(\zeta) + A_i \cosh b_i Z_i + B_i \sinh b_i Z_i \tag{7}$$

where $\zeta = z/\ell_3$, $L_i = \ell_i/\ell_3$, $b_i^2 = (U_i \ell_3/k_w)(S\ell_3/A_w)$, and $f_i(\zeta)$ and Z_i are summarized in Table 3. The zonal constants of integration, A_i and B_i, must be evaluated from the boundary and zonal matching conditions; explicit expressions are given in Ref. 6.

The mean-value theorem is used to integrate Eq. (5) and obtain an expression for the condensation front $L_c = \ell_c/\ell_3$:

Very low heat loads, $0 < \ell_c \le \ell_1$:

$$L_c = \frac{\bar{\psi}_r(V_r/V_c) + \bar{\psi}_1 L_1 + \bar{\psi}_2(L_2 - L_1) + \bar{\psi}_3(1 - L_2) - (m_g R_g/V_c)}{(\bar{\psi}_1 - \bar{\psi}_0)} \tag{8a}$$

Low-to-full heat loads, $\ell_1 < \ell_c \le \ell_2$:

$$L_c = \frac{\bar{\psi}_r(V_r/V_c) + (\bar{\psi}_0 - \bar{\psi}_1)L_1 + \bar{\psi}_2 L_2 + \bar{\psi}_3(1 - L_2) - (m_g R_g/V_c)}{(\bar{\psi}_2 - \bar{\psi}_1)} \tag{8b}$$

where

$$\bar{\psi}_i = \frac{p_v(T_e) - p_v(\bar{T}_i)}{\bar{T}_i}, \qquad \bar{T}_i = \frac{1}{\zeta'' - \zeta'} \int_{\zeta'}^{\zeta''} T_i(\zeta)\, d\zeta \tag{8c}$$

The mean temperatures follow from Eqs. (7) and (8c) in the form

$$\bar{T}_i = \bar{f}_i + \frac{1}{b_i W_i}[A_i \sinh b_i W_i + B_i(\cosh b_i W_i - 1)] \tag{8d}$$

where $\bar{f}_i$ and W_i are shown in Table 4.

The evaporator temperature follows from Eq. (7) with the assumption

$$T_e = T_0(0) = T_{s0} + q_0/U_0 + A_0 \tag{9}$$

where A_0 depends on the condensation front location L_c, the heat load Q, the geometry, and the several boundary and environmental conditions. In its simplest form, the performance problem is reduced to the simultaneous solution for T_e and L_c using Eqs. (8) and (9).

The formulation is complete for the very low-heat load case and has most of the characteristics of the first-order model of Ref. 1. The low-to-full heat load formulation is not complete because Eq. (4b) is not sufficient to define both q_0 and q_1. In principle, it is possible to use a one-dimensional vapor and liquid mass balance coupled with an enthalpy balance to evaluate condensation fluxes in the form

$$q_{\Delta\ell} = -\left(\frac{A_c M_v}{S(\ell'' - \ell')}\right)\left[\frac{HcD}{1-x}\left(\frac{dx}{dz}\right)_{z=\ell'} - \frac{HcD}{1-x}\left(\frac{dx}{dz}\right)_{z=\ell''}\right] \tag{10}$$

Real-gas properties (compressibility factor and diffusivity) for a high-pressure mixture of a polar (NH_3) and nonpolar (N_2) gas were taken from Ref. 7 in an attempt to incorporate Eq. (10) in the formulation. The approach proved unsuccessful; it appears that a two-dimensional analysis[8,9] is required to formulate expressions for the local condensation flux.

Despite the lack of a fully deterministic set of equations, an heuristic approach, based on the boundedness of q_0 and L_c, together with an independent constraint on the axial temperature gradient in condensing zones, was found to converge to a simultaneous solution for T_e, L_c, and q_0. The approach requires double iteration with respect to q_0 and L_c, and is described following the discussion of model validation.

Validation Analysis

In Ref. 1, the validation analysis proceeded in three distinct steps: 1) temperature profile matching, 2) semi-empirical estimate of heat-pipe void volume V_c, and 3) consistency check. These same steps were used here and are described briefly in the following section.

Temperature Profile Matching

The parameters in Table 2 were used as inputs to Eq. (7) to calculate axial temperature distributions for the three test runs. Systematic adjustments were made to the input set on a trial and error basis, until a "best fit" was found. The best-fit results did not require the use of Eq. (8). The test data and the best-fit results are shown in Fig. 2a. The adjustments were limited to the heat-loss coefficients through the foam insulation surrounding the transport sections and to the location of the condensation front; adjusted values of these parameters are shown in parentheses in Table 1. The variations are within the $\pm 10\%$ range expected for experimental studies. The analytical best fit does not match the test data precisely at the hot side of the condensation front, but the fit is acceptable for most applications. It is believed that the condensation flux is not uniform near the condensation front and continues "downstream" of the front location postulated by the present model. More significant than the axial temperature match is the close agreement between test data and analytical temperatures at the evaporator.

Estimate of Vapor Flow Cross Section and Noncondensable Gas Mass

The manufacturer provided data on the vapor/gas flow cross-section area and the mass of noncondensable gas. However, it was not possible to obtain agreement with those values with any one of the three best-fit results. It is believed that the combination of the bends in the pipe, the axially nonuniform wick geometry, and intrinsic uncertainties in the nominal values reported by the manufacturer make the nominal values inappropriate for the present application. Instead, the best-fit temperatures for runs U08 and U12 were used in Eqs. (8) to solve for "apparent" or "effective" values of A_c and m_g; a comparison of nominal and effective values is shown below:

Parameter	Nominal	Effective
Vapor/gas cross section A_c	3.206 E-6 m^2	5.642 E-5 m^2
Noncondensable gas mass m_g	3.921 E-3 kg	3.577 E-3 kg

The effective area approaches the geometric cross-section area of the clear pipe, 9.987 E-5 m^2; the effective gas mass is 9% less than the nominal value. The agreement between effective and nominal gas mass is improved if a compressibility factor[7] $Z = 0.89$ is introduced in the formulation. The order-of-magnitude disparity in vapor/gas cross section is believed to be due to the assumption of an isothermal reservoir; it was found that small changes in reservoir temperature caused large changes in A_c, while having very little influence on m_g.

Consistency Check

The effective values of A_c and m_g were used to solve for the condensation front L_c and the axial temperature distribution for run U13. The temperature distribution based on a gas mass balance is shown in Fig. 2a. The predicted evaporator temperature is approximately 0.8 K higher than the experimental value, and 0.69 K higher than the best-fit analysis. It is believed that the present model and the use of effective values for gas mass balance parameters is consistent and suitable for most engineering applications. Finally, the nominal values of m_g, A_c were used to solve for the pipe performance; the predicted evaporator temperature was found to be almost 5 K greater than the experimental value. Such a variance would not be acceptable for most design situations. In the absence of test data that may be used to find effective values of m_g and A_c, it appears necessary to use manufacturers' (nominal) values and to investigate the influence of reservoir temperature on VCHP performance.

This comparison of analytical and experimental results shows that a comparatively simple model of a VCHP may be used to predict performance for heat loads in the heat-load range 0–50% full load. These results complement the earlier findings[1]where a simpler model was found to be adequate in the range 20–100% full load. The earlier pipe[2] was a stainless steel/water/air VCHP without a supplementary gas reservoir and had a wick described as "200 mesh stainless steel, concentric annulus artery with two wraps of screen held in place by a spring." The present pipe is aluminum/ammonia/nitrogen with a moderate gas reservoir volume ($V_r/V_c \approx 3$); in the condenser and two transport sections, the wick is described as aluminum knitted mesh, central core, with spacers in the condenser. In consideration of the good agreement between experimental and analytical results for dissimilar VCHP's and heat loads, it is concluded that the one-dimensional fin model with constant zonal condensation fluxes is adequate for purposes of preliminary design and performance predictions.

Having established the credibility of the zero-to-full heat-load model and provided insights to the idiosyncrasies of the formulation, the next section presents a numerical example, identifies problems in using the double-flux equations, and compares the present model with the original model described in Ref. 1.

Numerical Example

The following example is based on environmental conditions observed during run U08. For purposes of illustration, the environmental temperature and heat-loss coefficients are postulated as being constant over the full range of heat loads. This assumption is made to minimize the number of parameters occurring in the problem; in a more realistic problem, the boundary temperatures would be constant and independent of heat load, but the heat-loss coefficients would be a function of

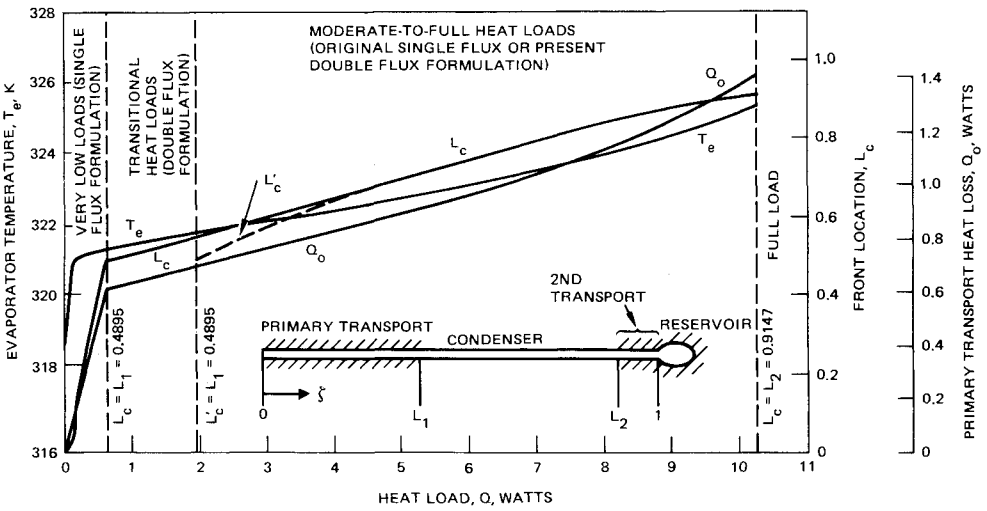

Fig. 4 Performance curves for hypothetical VCHP.

Table 5 Dimensions, properties, and parameters for hypothetical VCHP

Materials	
Pipe	6061T6 aluminum
Reservoir	304L stainless steel
Working fluid	NH_3, anhydrous ammonia
Noncondensable gas	N_2, high-purity nitrogen
Geometry	
Pipe o.d. × wall thickness × length	1.27 × 0.071 × 201.68 cm
Evaporator length	52.1 cm
Primary transport length	$\ell_1 = 73.8$ cm
Condenser length	$\ell_2 - \ell_1 = 64.14$ cm
Secondary transport length	$\ell_3 - \ell_2 = 12.85$ cm
Pipe circumference	$S = 3.99$ cm
Conduction cross section	$A_w = 0.2679$ cm^2
Vapor cross section	$A_c = 0.5643$ cm^2
Reservoir surface area	$A_r = 157.9$ cm^2
Reservoir volume	$V_r = 252.4$ cm^3
Thermal coefficients	
Pipe thermal conductivity	$k_w = 171.3$ W/m-K
Primary transport section	$U_0 = 6.81$ W/m^2-K
Condenser section	$h_1 = h_2 = 10.90$ W/m^2-K
Secondary transport section	$U_3 = 6.81$ W/m^2-K
Reservoir	$U_r = 11.36$ W/m^2-K
Gas charge	
Mass	$m_g = 3.577 \times 10^{-3}$ kg
Gas constant	$R_g = 0.2968$ kJ/kg-K
Vapor pressure	
Temperature coefficients (based on K)	$D_0 = -48.05$ $D_1 = 0.68546$ $D_2 = -3.3219 \times 10^{-3}$ $D_3 = 8.7447 \times 10^{-6}$ $D_4 = -1.2019 \times 10^{-8}$ $D_5 = 6.7905 \times 10^{-12}$ $C = 1.0$ Pa
Boundary temperatures	$T_{s0} = 318.3$ K $T_{s1} = T_{s2} = T_{s3} = T_{sr} = 293.6$ K

both surface and boundary temperatures. In the interests of simplicity and convenience, it is assumed that the reservoir is unheated, i.e., $Q_r = 0$. All of the information required to make performance predictions for the VCHP is summarized in Table 5.

The performance of this heat pipe is shown in Fig. 4. The heat load Q is the power entering the primary transport section from the evaporator; Q_0 represents the condensation loss in the primary transport section. In Fig. 4, L_c is the location of the condensation front, and T_e is the dependent variable of major interest to a VCHP user. Q_0 and L_c are usually of secondary interest, but in the present formulation, the magnitude of L_c is important to establish the set of coefficients that must be used to find T_e and Q_0. The heat loss Q_0 is important in the present instance because it must be found by double iteration when the double-flux formulation is used. In a broader sense, Q_0 also should be of interest to a VCHP user because it represents an uncontrolled loss. In many cases, if Q_0 is not taken into account, the VCHP may not achieve its expected performance.

The resolution of the VCPH performance problem requires a simultaneous solution for T_e, L_c, and $Q_0 = q_0 S\ell$ ($0 < \ell \leq \ell_1$) as functions of Q with parameters including geometry, environment, and thermophysical properties. Equations (9), (8), (6), and expressions for the several coefficients (A_i, B_i) and various defining equations [f_i, λ_3, $p_v(T)$, etc.] were programmed for execution by an Apple IIe computer. A user-interactive algorithm was developed in which calculations were initiated by estimating Q_0 and L_c. It was expedient to start by specifying $L_c = L_1$ to seek the heat load $\tilde{Q} = Q_0$ and the corresponding evaporator temperature. This required iterating only with respect to Q and observing L_c until the output satisfied L_c (out) $= L_1$. With $\tilde{Q}$ established, it follows that for $Q < \tilde{Q}$, then $Q_1 = 0$ and $L_c < L_1$; in this domain, single iteration with respect to L_c[1] yielded the evaporator temperature. For $Q > \tilde{Q}$, it followed that $Q_1 > 0$ and $L_c > L_1$. It was expedient next to seek the full-load condition corresponding to $L_c = L_2$; a trial value of Q was specified and iteration with respect to Q_0 proceeded either until L_c (out) $= L_2$, or it became apparent that no solution existed. For the latter condition, Q and Q_1 iteration continued until a value $Q = Q_{\text{full}}$ was found that yielded L_c (out) $= L_2$. The indeterminacy of the relationship between Q_0 and Q_1 required an additional criterion to verify the performance prediction for $Q = Q_{\text{full}}$.

The Second Law of Thermodynamics requires that the maximum temperature occur in the evaporator. This constraint is substantiated by the empirical observation that the heat-pipe temperature decreases monotonically with distance from the evaporator. This condition translates into the constraint $dT/dz \leq 0$ for $0 < z < \ell_3$ ($Q_r = 0$); specifically, it was found that the full-load solution must satisfy both L_c (out) $= L_2$ and $dT_0/dz < 0$ (i.e., $A_0 < 0$). The additional criterion was found to provide consistent performance predictions for all heat loads in the range $\tilde{Q} < Q \leq Q_{\text{full}}$. With the bounding heat loads $\tilde{Q}$ and Q_{full} established, it was reasonably straightforward to solve for the intermediate performance conditions; Q was specified, trial values of Q_0 and L_c (in) were selected, and L_c (out) was calculated. Double iteration with respect to Q_0 and L_c was continued until both L_c (out) $= L_c$ (in), and $A_0 < 0$ were satisfied.

The earlier single-flux formulation[1] was examined to establish its functional domain in Q. The earlier model postulated true adiabatic transport sections so that $Q_0 = 0$. This condition was introduced in the present model setting (Q_0,

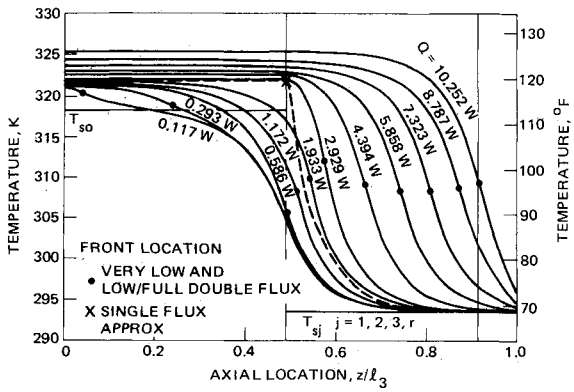

Fig. 5 Axial temperature distributions for hypothetical VCHP.

$U_0) = (0, 0)$ and seeking performance solutions in $\tilde{Q} < Q' \leq Q_{\text{full}}$ with $L_1 < L'_c \leq L_2$. Single iteration with respect to L' [Eq. (8b)] leads to a solution for $T'_e = T_0(L_1) = T_0(0)$ for a specified value to $Q' = Q_1$. Following this determination, an ancillary calculation was made to find the heat loss from the nonadiabatic primary transport section by restoring the surface-loss coefficient $U'_0 > 0$ to obtain $Q'_0 = U'_0 S\ell_1(T'_e - T_{s0})$. This sequence yielded the total heat load entering at $z = 0$ in the form $Q = Q'_0 + Q_1$.

The VCPH performance resulting from this post-hoc correction for heat load was found to yield values of T'_e and Q'_0 numerically identical to T_e and Q_0 found by the double-flux, double-iteration algorithm. The single-flux results deviate from the double-flux results only insofar as L'_c results from Eq. (8b) instead of L_c. The single-flux formulation ceases to be appropriate when it predicts $L'_c < L_1$; the dotted line in Fig. 5 shows the deviation between L_c and L'_c, and the lower limit is shown as $Q = Q_t = 1.933$ W. This numerical study suggests that the earlier single-flux formulation with a post-hoc correction and the present double-flux formulation yield equivalent values of T_e for heat loads in the range 20–100% of full load.

In Fig. 4, the operating heat-load range is subdivided into three regions:

Very low-heat load:

$$0 < L_c \leq L_1,\ 0 < Q \leq \tilde{Q} = 0.609 \text{ W}$$

Transitional heat loads:

$$L_1 < L_c < L_t,\ \tilde{Q} < Q < Q_t = 1.933 \text{ W}$$

Moderate-to-full loads:

$$L_t < L_c \leq L_2,\ Q_t < Q < Q_{\text{full}} = 10.252 \text{ W}$$

where L_t must be found from the double-flux formulation after establishing Q_t as the corrected lower bound of the earlier single-flux formulation. The transitional range is the only region that requires the double-flux formulation to predict T_e; single-flux analyses may be used for both very low-heat loads and moderate-to-full heat-load calculations.

The performance curves of Fig. 4 show that in each of three subregions (very low, transitional, moderate-to-full heat loads), the dependent performance variables T_e, L_c, Q_0 vary as near linear functions of heat load. This observation suggests that simple interpolation may be used to estimate the dependent variables from values obtained at Q, Q_t, and Q_{full}. In any case, linear interpolation may be used to obtain first estimates for Q_0 and L_c when double iteration is required to calculate VCHP performance.

Axial temperature distributions over the full length of the pipe, $0 < (z/\ell_3) \leq 1.0$, are shown in Fig. 5 for selected values of heat load. These temperature profiles were calculated with the double-iteration algorithm. The single dashed line for $Q = 1.933$ W represents the temperature distribution for the lower limit of the original single-flux formulation.[1] The circles designate the temperatures and locations of the condensation front L_c; the " × " on the dashed line shows the condensation front $L'_c = L_1$. The two temperature distributions for $Q = 1.933$ W share only a superficial similarity, but they predict virtually identical evaporator temperatures. Although not shown in Fig. 5, as Q increases above the transitional limit, $Q = Q_t = 1.933$ W, the temperature distributions found from the double-flux and single-flux formulations become more similar and indistinguishable for heat loads in the range $4.39 < Q \leq 10.25$ W.

Finally, numerical experiments[6] performed while developing the double-iteration formation showed that T_e is rather insensitive to the assumed value of Q_0. For example, with $Q = Q_0 + Q_1 = 1.757$ W, it was found that a $\pm 5\%$ variation in Q_0 ($= 0.680$ W) led to L_c (output) $= (1.0 \pm 0.05)\ L_c$ (output); however, the corresponding variation in T_e ($= 321.7$ K) was less than ± 0.6 K. This benign behavior may be used to advantage when establishing convergence criteria for computer codes.

Discussion

The work reported here is meaningful for both its experimental and analytical aspects. The test data should be useful to other researchers seeking to understand the thermal processes inside a VCHP. The heat-balance results summarized in Table 1 also should caution heat-pipe users of the importance of heat losses from insulated zones; it should be apparent that makeshift instrumentation and analytically intractable environmental conditions can lead to erroneous conclusions about the performance capability of a heat pipe. Additionally, the experimental axial temperature distribution given here may be used by other thermal analysts to evaluate various simplified models (e.g., flat-front models[5]) for VCHP performance prediction.

The analytical formulation, also, should be of interest to researchers and analysts. The extended model presented here provides unexpectedly good performance predictions and axial temperature distributions despite its neglect of seemingly important physical principles. Additional study is required to eliminate the indeterminacy of q_0 and q_1. The boundedness of q_0 and L_c and the constraint on dT/dz prevent the indeterminacy from being debilitating; however, the need for double iteration is irksome. It may be possible to find an entropy principle to evaluate q_0 (or q_1) while retaining the one-dimensional model. Alternatively, two-dimensional analyses[7,8] could be extended to include axial conduction in both wick and wall to provide a determinate basis for specifying condensation fluxes. Other features that require investigation include the model of the reservoir, improvement of the gas mass balance accuracy, and a formulation to include heat overloads that induce condensation in the secondary transport section and the gas reservoir.

The present study suggests that VCHP performance predictions are insensitive to the assumptions of zonal flux uniformity; radially isothermal vapor, gas, and structure; and neglect of axial conduction in the wick. On the other hand, the analytical model was found to be sensitive to the assumptions of an ideal gas ($Z = 1$) and an isothermal gas reservoir. This sensitivity was observed when test data were used to calculate the gas charge and the gas-vapor flow cross section. Insofar as gas charge and flow cross-section data are not always provided by heat-pipe manufacturers, the user will need to obtain data by experimental means. The assumption of an isothermal reservoir may prove to be tenable only when semi-empirical values of gas mass and flow cross-section area are available.

The apparent insensitivity of evaporator temperature to gas mass balance deserves further emphasis. In the numerical example above, it was found that a variation of $\pm 5\%$ in transport section heat loss, plus a comparable variation in the location of the condensation front, resulted in less than a ± 0.6 K variation in predicted evaporator temperature. These variations were accompanied by nonmonotonic axial temperature distributions, but their influence on performance was very small. Presumably, "flat-front" models also provide reasonable performance predictions despite the assumption of no

gas in the transport section or active condenser. This discussion is intended to point out the need for additional studies, both analytical and experimental, to define the circumstances in which all aspects of energy and mass conservation are important to the problem of performance prediction in a VCHP.

Conclusions

The following conclusions are based on a combination of experimental test data, numerical experiments, and analytical observations:

1) For very low heat loads, the condensation front occurs in the primary transport section ($0 < L_c \leq L_1$) and the performance set (Q, L_c, T_e) is dominated by heat leaks along the length of the primary transport section. A single-flux model is required to calculate performance.

2) For moderate-to-full heat loads, the condensation front occurs in the mid-to-far section of the condenser, and the performance is dominated by the heat loss from the condenser section. The simple model of Ref. 1 may be used to calculate performance when proper account is taken of losses in the primary transport section.

3) For low-to-moderate heat loads, the condensation front occurs in the near-to-midsection of the condenser, and the performance depends on heat losses from both the primary transport and condenser sections. The double-flux model developed here may be used for performance predictions.

4) Evaporator temperature is not a strong function of the analytical model insofar as different models are capable of providing predictions that are suitable for many thermal design purposes.

Finally, it is important to recognize the role of heat leaks in the primary transport section; in the numerical example, the heat leak was approximately 14% of the total for full-load operation and 100% of the total load for very low-load operation. This aspect of VCHP performance is significant when manufacturer's test data taken in a "leaky" environment is not corrected for spacecraft applications where multilayer blankets provide more effective insulation of adiabatic sections.

References

[1]Bobco, R. P., "Variable Conductance Heat Pipes: A First Order Model," *Journal of Thermophysics and Heat Transfer*, Vol. 1, Jan. 1987, pp. 35–42.

[2]Edwards, D. K. and Marcus, B. D., "Heat and Mass Transfer in the Vicinity of the Vapor-Gas Front in a Gas Loaded Heat Pipe," *Journal of Heat Transfer*, Vol. 94C, No. 2, May 1972, pp. 155–162.

[3]Chapman, A. J., *Heat Transfer*, Macmillan, Oxford, England, UK, 1974, p. 382.

[4]Delil, A. A. M. and van der Vooren, J., "Uniaxial Model for Gas Loaded VCHP Performance in the Inertial Flow Regime," *Advances in Heat Pipe Technology*, edited by D. A. Reay, third ed., Pergamon Press, New York, pp. 359–372.

[5]Brennan, P. J. and Kroliczek, E. J., *Heat Pipe Design Handbook*, NASA NAS5-23406, June 1979.

[6]Bobco, R. P., "An Extended Model for Variable Conductance Heat Pipe (VCHP) Analysis: Zero-to-Full Heat Loads," AIAA Paper 87-1614, June 1987.

[7]Hirschfelder, J. O., Curtiss, C. F., and Bird, R. B., *Molecular Theory of Gases and Liquids* (corrected printing with notes added), Wiley, New York, 1954.

[8]Rohani, A. A. and Tien, C. L., "Steady Two-Dimensional Heat and Mass Transfer in the Vapor-Gas Region of a Gas Loaded Heat Pipe," *Journal of Heat Transfer*, Vol. 95, Aug. 1972, pp. 377–382.

[9]Hijakata, K., Chen, S. J., and Tien, C. L., "Noncondensable Gas Effect on Condensation in a Two-phase Closed Thermo-syphon," *International Journal of Heat Transfer*, Vol. 27, Aug. 1984, pp. 1319–1325.